Notice to Data Users: The documentation for this data set was provided solely by the Principal Investigator(s) and was not further developed, thoroughly reviewed, or edited by NSIDC. Thus, support for this data set may be limited.

Daily Global Land Parameters Derived from AMSR-E and AMSR2 (Version 2.0)

Contact Information:
Jinyang Du, John S. Kimball and Lucas A. Jones
Numerical Terradynamic Simulation Group (NTSG)
The University of Montana
Missoula MT, 59812

Email:
jinyang.du@ntsg.umt.edu; johnk@ntsg.umt.edu; lucas@ntsg.umt.edu

URL:
https://daacdata.apps.nsidc.org/pub/DATASETS/nsidc0451_AMSRE_Land_Parms_v02/

Document last updated: 09/01/2017 with minor edits by NSIDC

Table of Contents

I. Data introduction 2
II. LPDR changes from prior versions 3
III. Algorithm description 3
IV. Data File Information 4
V. File naming convention 5
VI. LPDR accuracy and performance 6
VII. Data version 13
VIII. Data citation, acknowledgements and references 13

I. Data introduction

The Version 2 global land parameter data record (LPDR) was generated using calibrated microwave brightness temperature (T_b) records from the Advanced Microwave Scanning Radiometer for EOS (AMSR-E) on the NASA EOS Aqua satellite, and the Advanced Microwave Scanning Radiometer 2 (AMSR2) sensor on the JAXA GCOM-W1 satellite. JAXA AMSR2 L1R orbital swath T_b retrievals were calibrated against similar RSS (Remote Sensing Systems) Version 7 AMSR-E T_b records, where individual T_b frequencies and ascending and decending orbit retrievals were calibrated separately (Du et al. 2014). The daily multi-frequency, ascending and decending orbit, and vertically and horizontally polarized T_b records extend from Jun. 19, 2002 to Dec. 31, 2015 and were used as primary inputs to an iterative retrieval algorithm for simultaneous estimation of a set of higher order land parameters (Du et al. 2017). The resulting land parameter record includes 30-day temporally smoothed fractional open water cover *(fw)* and daily (non-smoothed) fractional open water *(fwns)* estimates*;* daily surface air temperature minima and maxima (T_{mn} and T_{mx}, ~2 m height); X-band (10.7 GHz) vegetation optical depth (*VOD*); surface (10.7 GHz) volumetric soil moisture (*vsm*); and atmosphere total collumn precipitable water vapor (*V*). The resulting LPDR is available in a 25-km resolution global EASE-Grid (v1) projection. The global retrievals are affected by land cover conditions within the sensor footprint used for generating 25 km gridded resolution T_b record; the land parameter estimates were only carried out over land for classified non-precipitating, snow and ice free conditions. Accordingly, ancillary quality control (QC) bit flag files were also generated recording the average land coverage within each 25 km grid cell and indicating other quality factors,

including non-retrieval conditions for missing T_b observations, snow cover, rain, and identified radio frequency interference (RFI) in the 10.7, and 18.7 GHz channels.

The LPDR Version 2 (v2) data are aimed to provide an enhanced data record over prior (v1) LPDR releases in terms of both retrieval accuracy and temporal coverage. The LPDR v2 record provides consistent land parameter retrievals spanning both AMSR-E and AMSR2 (AMSR-E/2) operational records, and are suitable for science quality evaluations of key land parameters important to ecosystem processes.

II. LPDR changes from prior versions

The LPDR v2 data record effectively replaces prior LPDR releases. The v2 record extends the global land parameter observations from AMSR-E to AMSR2, enabling LPDR continuity from continuing AMSR2 operations. The v2 record also reflects numerous algorithm refinements and performance enhancements benefitting from ongoing calibration, validation and science application studies. A detailed description of the LPDR v2 algorithms and changes are provided elsewhere (Du et al. 2017), while major v2 refinements and updates from prior (v1) LPDR releases are summarized below and in Section II:

- The LPDR is derived from calibrated T_b retrieval records from both AMSR-E and AMSR2, allowing continuity of the data record, which extends from Jun. 19, 2002 to Jun. 30, 2017 for Version 2;
- The *V* algorithm is refined by additional accounting of cloud liquid water and surface terrain effects; and improved by calibrating against similar retrievals from the Atmospheric Infrared Sounder (AIRS).
- A refined estimation of T_{mx} and T_{mn} that considers terrain and latitude effects;
- An improved X-band (10.7 GHz) *vsm* retrieval using a weighted averaging strategy and dynamic selection of vegetation scattering albedo effects.

III. Algorithm description

The Version 2 algorithm was derived based on the general framework of the Version 1 algorithm (Jones et al., 2010) and later algorithm revisions (Du et al., 2015, 2016, 2017).

The LPDR v1 algorithms first derive effective surface temperature (*Ts*), T_{mx} and T_{mn}, *fw* and *V* using an iterative algorithm approach that incorporates H- and V-polarized 18.7 GHz and 23.8 GHz T_b data and several temperature insensitive microwave indices (Jones et al., 2010). The X-band (10.7 GHz) *VOD* is then obtained by inverting the land-water microwave emissivity slope index, and surface (~ 0-1 cm depth) *vsm* is acquired after correcting for X-band atmosphere, *fw* and vegetation effects (Jones et al., 2010). Different from other available AMSR-E algorithms, the methodology exploits satellite multi-

frequency T_b observations for synergistically retrieving multiple inter-connected land parameters; and specifically accounts for the impacts of land surface open water on the *V*, T_{mx} and T_{mn} , *VOD* and *vsm* retrievals (Jones et al., 2010; Du et al., 2017).

The Version 2 algorithm refinements include: (a) an empirical calibration of the AMSR (AMSR-E and AMSR2) derived estimation for *V* based on similar observations from AIRS (Du et al., 2015); (b) the T_b screening under frozen land surface conditions identified using an existing global daily freeze-thaw (FT) data record derived from a refined classification algorithm (Kim et al., 2017); (c) improved AMSR estimations of T_{mn} and T_{mx} that considers terrain and latitude effects (Du et al., 2015); (d) refined AMSR-E X-band (10.7 GHz) *vsm* retrievals using a weighted averaging strategy and dynamic selection of vegetation scattering albedo effects (Du et al., 2016) and (e) an empirical *fw* calibration made for improving the *vsm* inversion (Du et al., 2017). To account for the differences between RSS V7 and V6 AMSR-E T_b retrievals which were separately used in Version 2 and Version 1 algorithms, values of the following empirical parameters including reference dry soil emissivities, reference pure water emissivities, and delta parameter for descending orbits were adjusted from the original values in (Jones et al., 2010). Accordingly, regressions were re-made for estimating *V* , T_{mn} and T_{mx} based on pre-defined procedures as detailed in (Du et al., 2017). In addition, for producing a consistent LPDR spanning the AMSR-E to AMSR2 observation periods, AMSR2 T_b data were empirically inter-calibrated against AMSR-E based on similar overlapping FY3B MWRI satellite sensor observations (Du et al., 2014). The gridded AMSR T_b data were calculated from overlapping sensor footprints using an Inverse Distance Weighting interpolation method.

IV. Data File Information

The LPDR data files are provided in GeoTIFF (.tif) format. Each daily file contains a 3-D array (6 bands×1383 columns × 586 rows) of 32-bit float-type data containing all of the retrieved land parameters. The data are projected into 25 km global EASE-Grid (v1) format. The fill value is -999.0. Detailed data band information is described below:

Table 1. LPDR data band description

Band name	Parameter	Descriptions	Unit	Valid range
Band 1	*fw*	Non-smoothed open water fraction	dimensionless	0-1
Band 2	*fwns*	30-day smoothed open water fraction	dimensionless	0-1
Band 3	T_{mn} *or* T_{mx}	Daily surface air temperature minima or maxima, corresponding to descending or ascending pass retrievals	Kelvin	240- 340
Band 4	*V*	Vertically integrated atmospheric water vapor	mm	0-80
Band 5	*VOD*	Vegetation optical depth at 10.7 GHz	Neper	0-3
Band 6	*vsm*	Volumetric soil moisture at 10.7 GHz	cm^3/cm^3	0-1

Additional bit-wise data quality files (QA) are provided in GeoTIFF (.tif) format for describing the quality information of LPDR data files. Each QA file corresponding to a LPDR data file contains a 2-D array (1383 columns × 586 rows) of 8-bit byte-type data. The data are projected into 25 km global EASE-Grid (v1) format. The fill value is 255. Detailed quality flag descriptions are listed below:

Table 2. LPDR data quality flag descriptions

Bit number	Land surface condition	Indication
1st	Frozen ground	No LPDR retrieval
2nd	Snow or ice presence	No LPDR retrieval
3rd	Strong precipitation	No LPDR retrieval
4th	RFI at 18.7 GHz	No LPDR retrieval
5th	RFI at 10.65 GHz	No LPDR retrieval
6th	Dense vegetation with *VOD* > 2.3	Larger retrieval uncertainty
7th	Large water bodies with *fw* > 0.2	Larger retrieval uncertainty
8th	Saturated microwave signals with V-pol and H-pol Tb difference at 18 GHz or 23 GHz less than 1.0 K	Larger retrieval uncertainty

V. File naming convention

LPDR data file

AMSRU_Mland_{year}{day of year}{overpass (A or D)}_v#.tif

The string "AMSRU_Mland" represents global land parameters derived from both AMSR-E and AMSR2 observations. The year string contains four digits. The day-of-year is the day in three digits since January 1 of the year. The overpass character is either 'A' for ascending (afternoon; P.M.) or 'D' for descending (morning; A.M.). The v# indicates the data set version. The file extension "tif" is associated with the GeoTIFF file type.

QA file

AMSRU_Mland_{year}{day of year}{overpass (A or D)}_QA_v#.tif

The QA files share the same naming convention with the LPDR data files except an additional descriptor "_QA" is added. The v# indicates the data set version.

VI. LPDR accuracy and performance

A detailed LPDR (v2) accuracy and performance assessment was conducted over the global domain and is summarized elsewhere (Du et al. 2017). A summary of LPDR performance for the primary land parameters is provided below.

Fractional open water

The AMSR-E (year 2010) and AMSR2 (year 2015) *fw* summer composites were compared with a finer spatial resolution static water map derived from MODIS-SRTM (MOD44W) observations. Both AMSR-E and AMSR2 results (Fig.1a, 1b) captured a similar global inundation pattern as MOD44W (Fig.1c) including major river systems such as the Amazon River and Yangtze River, and widespread inundation occurring within pan-Arctic region. Quantitative comparisons of LPDR *fw* summer means over the globe for years 2003 to 2010 and representing the AMSR-E full-year observation record and AMSR2 observations from 2013-2015 in relation to MOD44W are summarized in Table 3. The resulting LPDR *fw* summer averages show overall favorable spatial correspondence with the MOD44W *fw* map ($R \geq 0.75$ and $RMSE \leq 0.06$). The AMSR2 portion of the LPDR shows an overall higher performance than AMSR-E, which may result from improved AMSR2 sensor footprint resolution relative to AMSR-E, enabling better land surface delineation.

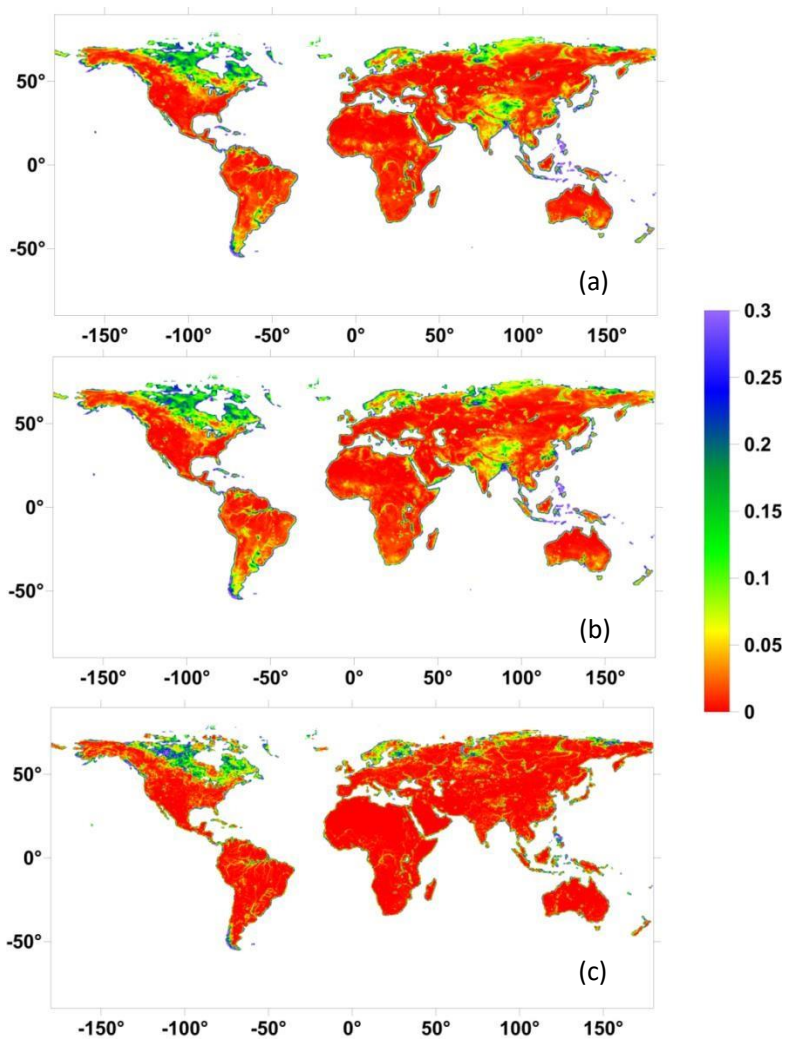

Fig.1 Summer composite (JJA) of 25-km global fractional water over land retrieved from AMSR-E ascending observations for year 2010 (a); AMSR2 ascending observations for year 2015 (b); and 25-km MOD44W static water map aggregated from original 250-m resolution (c).

Table 3. Comparisons of fw global averages over AMSR-E (2003-2010) and AMSR2 (2013-2015) periods in relation to the MOD44W static open water map. All products were projected into a consistent 25.0 km resolution EASE-GRID format; positive and negative bias indicates fw over- and under- estimation, respectively, relative to the static water map

AMSR-E/2 *fw* vs MOD44W						
	R*		RMSD*		Bias	
	Asc*	Dsc*	Asc*	Dsc*	Asc*	Dsc*
AMSR-E	0.767	0.750	0.057	0.057	0.016	0.012
AMSR2	0.795	0.775	0.054	0.054	0.017	0.013

* R denotes Pearson correlation coefficient; RMSD denotes Root Mean Square Difference; Asc and Dsc denote respective ascending and descending orbits.

Total precipitable water vapor and daily maximum/minimum air temperature

The resulting spatial distributions of V (Fig. 2) and T_{mx} (Fig. 3) summer composites were generated for AMSR-E (year 2010) and AMSR2 (year 2015) based on their daily ascending orbit retrievals. Similar to the previous results (Du et al., 2014), the V retrievals show a latitudinal gradient with higher values at lower latitudes and warmer regions consistent with the near-exponential relationship between atmospheric temperature and moisture holding capacity, except for dry desert regions distinguished by characteristicly lower V levels. The T_{mx} distributions also follow a similar latitudinal gradient as V but with more complex spatial variations affected by regional climate, land cover conditions and elevation gradients (Du et al., 2015).

The LPDR V and air temperature retrievals were quantitatively validated against NASA Aqua AIRS observations and in-situ temperature measurements at 142 global WMO weather station locations for selected years 2010 and 2013 (Table 4). The AMSR retrievals show strong agreement with the AIRS V product ($R \geq 0.91$; RMSE ≤ 4.98 mm), though a slight V over estimation and under estimation is indicated for respective AMSR-E (bias $\leq$ 0.23 mm) and AMSR2 (bias $\geq$ -0.27 mm) portions of record (Table 4). The LPDR corresponded favorably with the WMO air temperature measurements ($R \geq 0.89$; RMSE $\leq$ 3.46 ºC). The AMSR-E (2010) and AMSR2 (2013) retrievals show similar T_{mn} and T_{mx} retrieval accuracy, with associated RMSE differences within 0.13 K in relation to the WMO daily temperature measurements. However, the calibrated AMSR2 T_b record is not identical to that of AMSR-E as reflected by a maximum 0.40 ºC difference in their T_{mx} and T_{mn} retrieval biases against WMO measurements (Table 4).

Table 4. LPDR daily T_{mx}, T_{mn} and ascending/descending orbit based V accuracy in relation to respective in-situ air temperature measurements and AIRS V observations for 142 global WMO site locations for selected years 2010 (AMSR-E) and 2013 (AMSR2).

	T_{mx} (ºC)			T_{mn} (ºC)		
	R	RMSE	Bias*	R	RMSE	Bias
AMSR-E	0.928	3.428	0.637	0.899	3.307	0.061
AMSR2	0.917	3.484	0.260	0.899	3.150	0.265
	V (mm) from Ascending Orbits			V (mm) from Descending Orbits		
	R	RMSE	Bias	R	RMSE	Bias
AMSR-E	0.926	4.241	0.266	0.923	4.788	0.197
AMSR2	0.914	4.473	-0.369	0.911	4.941	-0.050

*Bias is calculated from retrievals minus observations.

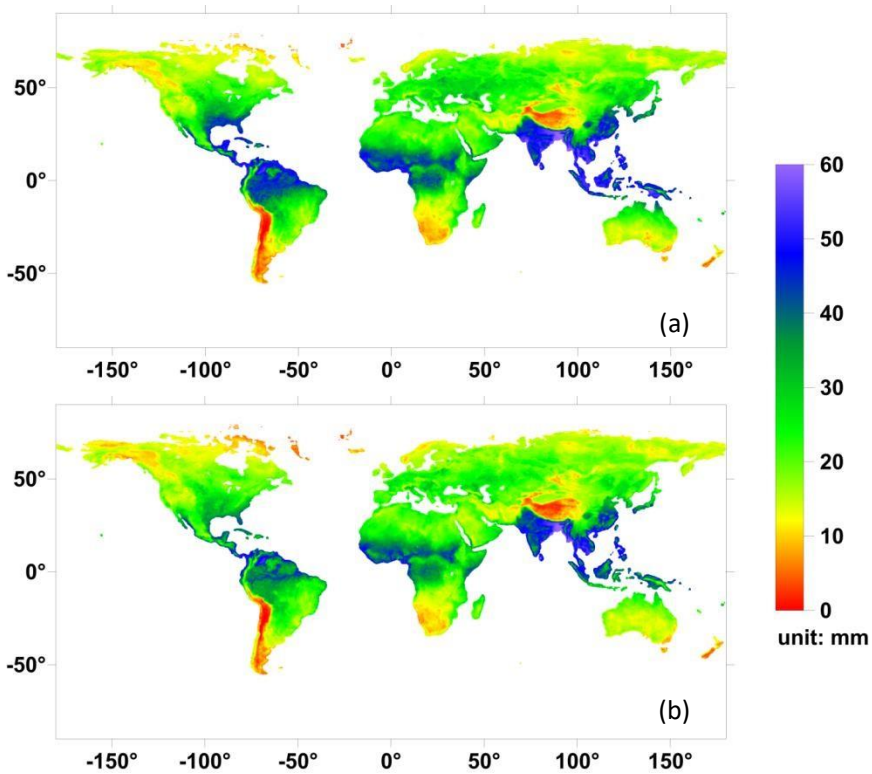

Fig.2 Summer composite (JJA) of 25-km precipitable water vapor (*V*, mm) over land retrieved from AMSR-E ascending observations for year 2010 (a); AMSR2 ascending observations for year 2015 (b).

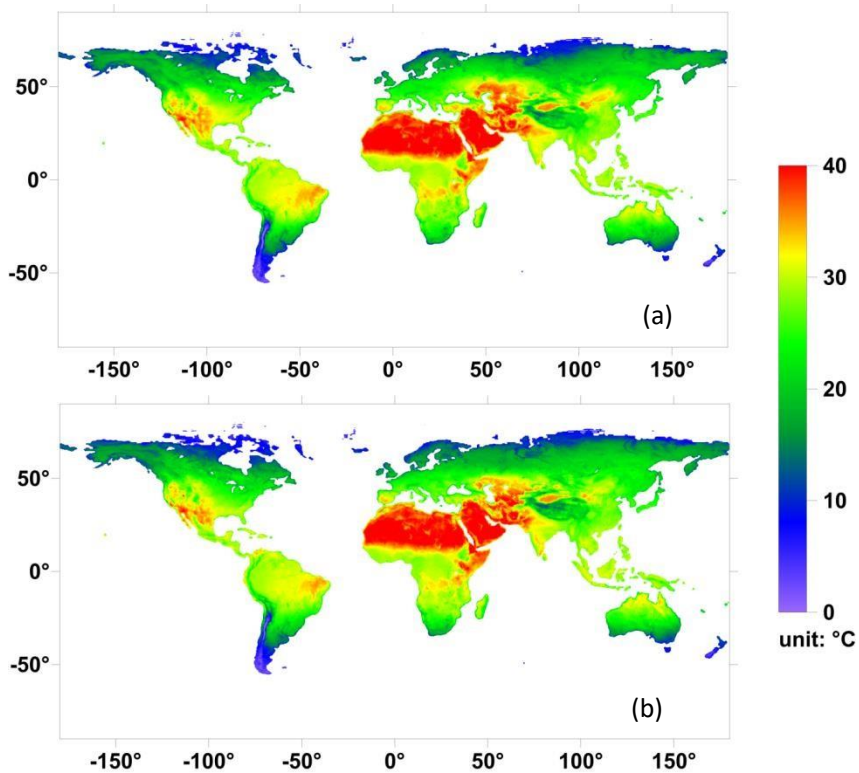

Fig.3 Summer composite (JJA) of 25-km global maximum daily surface air temperature (T_{mx}) over land retrieved from AMSR-E ascending observations for year 2010 (a); AMSR2 ascending observations for year 2015 (b).

Vegetation optical depth

The resulting spatial distributions of X-band (10.7 GHz) *VOD* Northern-Hemisphere summer composites (JJA) were generated for AMSR-E (year 2010) and AMSR2 (year 2015) based on their daily ascending orbit retrievals. Both AMSR-E and AMSR2 *VOD* retrievals from the LPDR show a similar global distribution pattern (Fig.4). Highest *VOD* values are found at rainforest regions including the Amazon Basin, Congo Basin and Southeast Asia, and high-latitude boreal forest regions; while the lowest *VOD* values are shown in desert or barren land areas such as the Sahara Desert, Taklamakan Desert, Sonoran desert and Central Australia. Moderate *VOD* values generally reflect median vegetation conditions of the regions including the grassland in the Central US, the Africa ecoclimatic transition zone Sahel and major rice fields in Central China and India. However, caution is needed when analyzing long-term *VOD* changes especially for higher biomass regions where AMSR T_b observations and *VOD* retrievals tend to get saturated and become more sensitive to the sensor inter-calibration accuracy (Du et al., 2017).

The LPDR derived *VOD* (10.7 GHz) was compared with the GIMMS3g NDVI climatology monthly means for the aggregate 2003-2010 and 2013 to 2015 observation record. Here, the mean seasonal cycle in *VOD* and NDVI is depicted for major IGBP global land cover types, including evergreen needleleaf forest (ENF), evergreen broadleaf forest (EBF), deciduous needleleaf forest (DNF), deciduous broadleaf forest (DBF), grassland and cropland. Both *VOD* and NDVI display similar seasonal cycles represented by their mean monthly time series ($R \geq 0.88$) (Table 5). Differences in NDVI correspondence between the ascending and descending orbit *VOD* records may reflect regional *VOD* retrieval uncertainties contributed by deficiencies in the underlying LPDR algorithm assumptions and parameterizations, which are discussed in (Du et al., 2017).

Table 5. Pearson correlations [R] between LPDR *VOD* (10.7 GHz) and GIMMS3g NDVI climatology monthly means for the aggregate 2003-2010 and 2013 to 2015 observation record. The comparisons were made for all global vegetation and selected land cover areas, including: ENF, EBF, DNF, DBF, grassland and cropland. Both products were projected into a consistent 25.0 km resolution EASE-GRID format. *VOD* results are delineated for LPDR ascending and descending orbit records**.**

Pearson correlation coefficient	Global	ENF	EBF	DNF	DBF	Grassland	Cropland
Ascending	0.878	0.715	0.218	0.893	0.201	0.903	0.665
Descending	0.937	0.898	-0.116	0.944	0.871	0.951	0.845

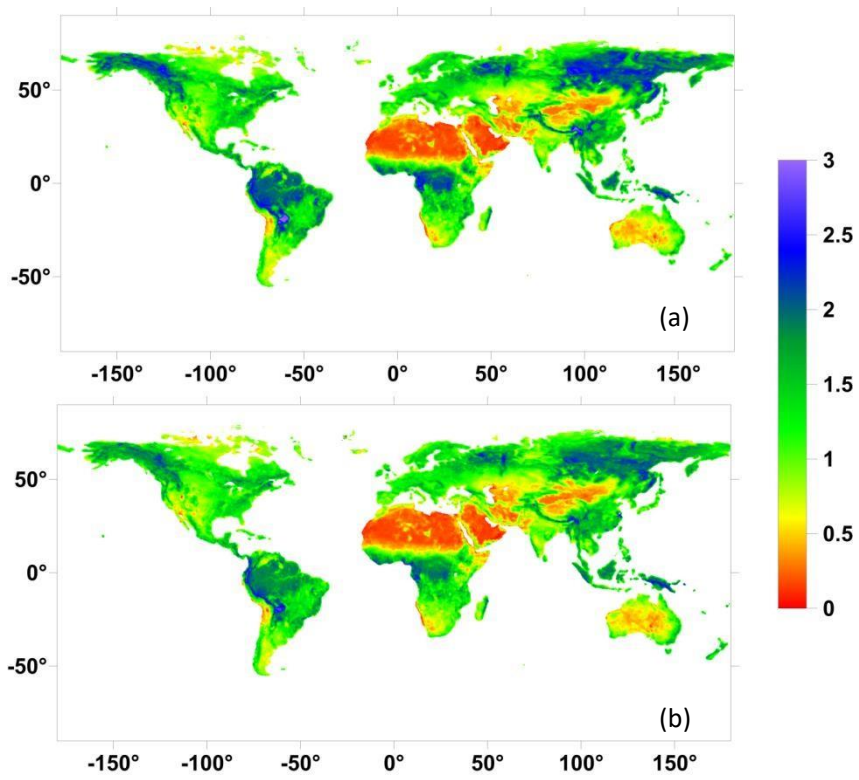

Fig.4 Summer composite (JJA) of 25-km global *VOD* (10.7 GHz) retrieved from AMSR-E ascending observations for year 2010 (a); AMSR2 ascending observations for year 2015 (b).

Soil Moisture

The AMSR soil moisture retrievals were compared against globally distributed validation watershed measurements as shown in Table 6. The overall retrieval accuracy is similar to that presented in (Du et al., 2016) with a general better performance of descending (AM) orbit retrievals than the ascending (PM) orbit observations. The global soil moisture distributions (Fig.5) derived from both AMSR-E and AMSR2 are similar to each other and consistent with the known global climatology including characteristically wet surface soil moisture conditions in northern high latitude areas, drier soil moisture extremes in deserts and semi-arid regions, such as the African Sahara desert, Southern California Desert, and central and western desert regions of Australia.

Table 6: Summary of satellite LPDR soil moisture retrieval accuracy in relation to in situ surface soil moisture measurements from four globally distributed validation watersheds.

Statistics	Little River (USA; 2003-2005)	Little Washita (USA;2003-2005)	Naqu (China; 2010-2011)	Yanco (Australia; 2009-2011)	All Sites*
		Ascending Orbits			
R	0.627	0.762	0.790	0.755	0.815
RMSE*	0.035	0.036	0.051	0.059	0.045
Bias	0.041	0.053	-0.102	-0.042	0.012
		Descending Orbits			
R	0.696	0.733	0.831	0.787	0.835
RMSE*	0.032	0.036	0.042	0.055	0.042
Bias	0.071	0.086	-0.063	-0.031	0.038

R is coefficient coefficient; RMSE (Root Mean Square Error) and Bias are in cm^3/cm^3. *RMSE and All Sites statistics except bias are calculated with watershed bias corrected.

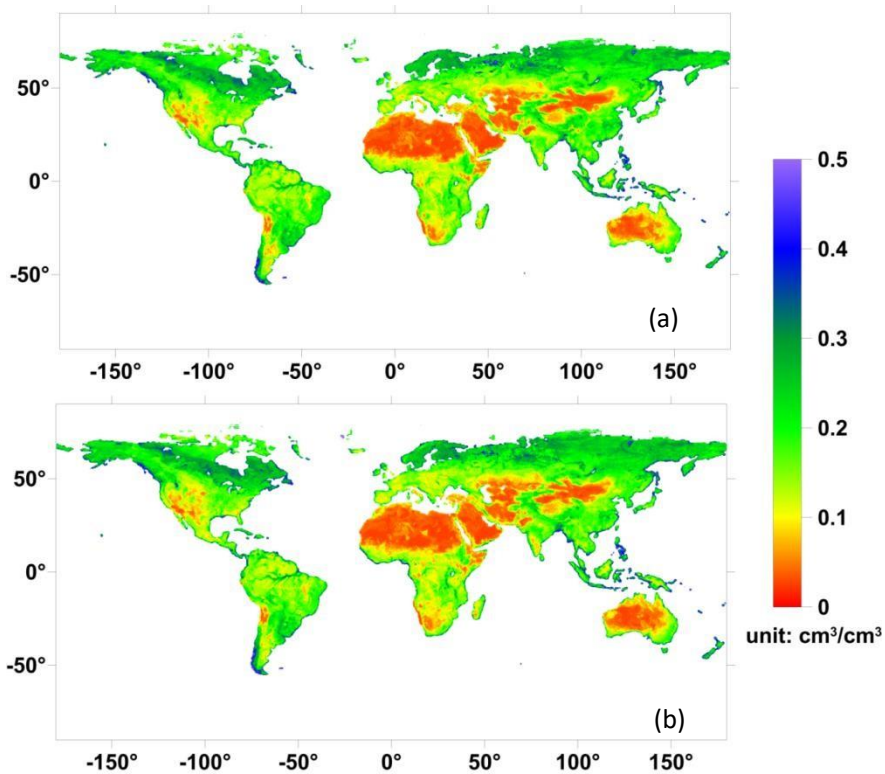

Fig.5 Summer composite (JJA) of 25-km X-band (10.7 GHz) global volumetric soil moisture (*vsm*) retrieved from AMSR-E ascending observations for year 2010 (a); AMSR2 ascending observations for year 2015 (b).

VII. Data version

Version 1

Original data released on 1/21/2010 followed by grid and flag updates on 9/12/2011 and data processed through the end of the AMSR-E record on 4/23/2012. The v1 algorithms and product performance are described in the literature (Jones et al, 2010).

Version 2

Data released on 3/22/2017 and updated on 8/27/2017. Data were processed for the entire AMSR-E operational record (06/19/2002 to 09/30/2011) and part of the AMSR2 record (07/24/2012 to 06/30/2017), with planned updates and LPDR continuity enabled from continuing AMSR2 operations. The associated v2 algorithms were revised from the prior v1 algorithm (Jones et al, 2010) as detailed in the literature (Du et al., 2014, 2015 and 2016) and summarized in (Du et al., 2017).

VIII. Data citation, acknowledgements and references

As a condition of using these data, you must cite the use of this data set using the following citation. For more information, see our Use and Copyright Web page:

Du, J., Jones, L. A. and J. S. Kimball. 2017. *Daily Global Land Surface Parameters Derived from AMSR-E and AMSR2, Version 2*. [Indicate subset used]. Boulder, Colorado USA. NASA National Snow and Ice Data Center Distributed Active Archive Center. doi: http://dx.doi.org/10.5067/RF8WPYOPJKL2. [Date Accessed].

As a condition of using these data, we request that you acknowledge the author(s) of this data set by referencing the following peer-reviewed publication:

Du, J., J.S. Kimball, L.A. Jones, Y. Kim, J. Glassy, and J.D. Watts. 2017. A global satellite environmental data record derived from AMSR-E and AMSR2 microwave earth observations. *Earth System Science Data* 9(2): 791-808. doi:10.5194/essd-9-791-2017.

Acknowledgements: These data were generated through a grant from the NASA MEaSUREs (Making Earth System Data Records for Use in Research Environments) program (NNX14AB20A). This work was conducted at the University of Montana under contract to NASA.

Other References are listed below:

[1] Kim, Y., Kimball, J. S., Glassy, J., and Du, J.: An Extended Global Earth System Data Record on Daily Landscape Freeze-Thaw Status Determined from Satellite Passive Microwave Remote Sensing, *Earth Syst. Sci. Data*., 9 (1), 133-147, 2017.

[2] Du, J.; Kimball, J.S.; Jones, L. A . Passive Microwave Remote Sensing of Soil Moisture Based on Dynamic Vegetation Scattering Properties for AMSR-E. *IEEE Transactions on Geoscience and Remote Sensing.* 2016, 54 (1), 597-608.

[3] Du, J., J.S. Kimball, and L.A. Jones. Satellite microwave retrieval of total precipitable water vapor and surface air temperature over land from AMSR2. *IEEE Transactions on Geoscience and Remote Sensing*, 2015, 53 (5), 2520-2531 (DOI 10.1109/TGRS.2014.2361344).

[4] Du, J.; Kimball, J.S.; Shi, J.; Jones, L.A.; Wu, S.; Sun, R.; Yang, H. Inter-Calibration of Satellite Passive Microwave Land Observations from AMSR-E and AMSR2 Using Overlapping FY3B-MWRI Sensor Measurements. *Remote Sens.* 2014, *6*, 8594-8616.

[5] Jones, L.A.; Ferguson, C.R.; Kimball, J.S.; Zhang, K.; Chan, S.T.K.; McDonald, K.C.; Njoku, E.;Wood, E. Satellite microwave remote sensing of daily land surface air temperature minima and maxima from AMSR-E. *IEEE J. Sel. Top. Appl. Earth Obs. Remote Sens*. 2010, 3, 111–123.